Singlet oxygen-based photoelectrochemical detection of miRNAs in prostate cancer patients' plasma : a novel diagnostic tool for liquid biopsy

Singlet oxygen-based photoelectrochemical detection of miRNAs in prostate cancer patients' plasma: a novel diagnostic tool for liquid biopsy

Saranya Thiruvottriyur Shanmugam [a, b], Rui Campos [a, b, 1], Stanislav Trashin [a, b], Elise Daems [a, b], Diogo Carneiro [c,d], Avelino Fraga [c,d], Ricardo Ribeiro [c,e] and Karolien De Wael [a, b*]

[a] *A-Sense Lab, Department of Bioscience Engineering, University of Antwerp, Groenenborgerlaan 171, 2020, Antwerp, Belgium*

[b] *NANOlab Center of Excellence, University of Antwerp, Groenenborgerlaan 171, 2020, Antwerp, Belgium*

[c] *i3S, Tumour & Microenvironment Interactions Group, Instituto de Investigação e Inovação em Saúde, University of Porto, Rua Alfredo Allen 208, 4200-135 Porto, Portugal*

[d] *Department of Urology, Centro Hospitalar Universitário do Porto, Largo Prof. Abel Salazar, 4099-001 Porto, Portugal*

[e] *Department of Pathology, Centro Hospitalar Universitário do Porto, Largo Prof. Abel Salazar, 4099-001 Porto, Portugal*

[1] *Current address: Food Quality and Safety Group, International Iberian Nanotechnology Laboratory (INL), Av. Mestre José Veiga, 4715-330 Braga, Portugal*

[*] *Corresponding author: karolien.dewael@uantwerpen.be*

ABSTRACT

Dysregulation of miRNA expression occurs in many cancers, making miRNAs useful in cancer diagnosis and therapeutic guidance. In a clinical context using methods such as polymerase chain reaction (PCR), the limited amount of miRNAs in circulation often limits their quantification. Here, we present a PCR-free and sensitive singlet oxygen ($^1O_2$)-based strategy for the detection and quantification of miRNAs in untreated human plasma from patients diagnosed with prostate cancer. A target miRNA is specifically captured by functionalised magnetic beads and a detection oligonucleotide probe in a sandwich-like format. The formed complex is concentrated at the sensor surface via magnetic beads, providing an interface for the photoinduced redox signal amplification. The detection oligonucleotide probe bears a molecular photosensitiser, which produces $^1O_2$ upon illumination, oxidising a redox reporter and creating a redox cycling loop, allowing quantification of pM level miRNA in diluted human plasma within minutes after hybridisation and without target amplification.

Keywords: Photoelectrochemistry, Singlet oxygen, Nucleic acids, miRNA

1. INTRODUCTION

Cancer remains the second leading cause of death globally, with a projected increase of 28.4 million new cancer cases in 2040, a 47% rise compared to 19.3 million cases in 2020 [1]. Such a burden can be reduced by detecting cancer at an early stage, effectively treating the patient and monitoring the response to the therapy. While early diagnosis leads to a greater chance of survival and less expensive treatment, screening individuals will help in identifying if the patient is at risk of developing cancer even before they develop symptoms. This is facilitated by liquid biopsies allowing to track biomarker levels for early diagnosis, screening through the disease course and treatment in a minimally invasive manner [2,3]. Liquid biopsy enables the detection of various cancer biomarkers such as circulating tumour cells, circulating tumour DNA, and non-coding microRNAs (miRNAs) [4–7]. In particular, the differential amount of miRNAs in circulation has been clinically associated with the cancerous site and tumour progression [8,9]. Moreover, the use of miRNA levels is promising to predict the chemotherapeutic response of an individual [10]. A striking example is the dysregulation of certain miRNAs associated with prostate cancer aiding in diagnosis and prognosis. An enhanced plasmatic expression of miR-141-3p [11,12] and miR-145-5p (hereafter called miR-141 and miR-145, respectively) is associated with prostate cancer progression and prognosis [13–16].

Currently, the standard techniques for detecting and quantifying miRNA are reverse transcription quantitative real-time PCR (RT-qPCR) and gene sequencing options (i.e. next-generation sequencing) [17–21]. While both techniques offer high sensitivity and reliable variant detection, the downsides of these techniques include high cost, complex sample preparation, risks of contamination, long analysis time and low miniaturisation potential which limits the use at the point of care (POC) testing [18,20,21].

Electrochemical and photoelectrochemical platforms offer rapid and sensitive analysis of miRNAs directly in biological samples with low concentrations of biomarkers and demonstrated great potential for POC due to technological advances in microelectronics and low-cost sensor transducers, i.e., disposable electrodes [22–27]. There are sufficient review articles in the literature offering a comprehensive overview of the current developments in electrochemical biosensors for miRNA and listing different approaches to the detection of miRNA [23,26,28–30]. Some notable articles include Sfragano et al. [26] summarising recent developments and approaches to overcome obstacles in miRNA detection, and Gillespie et al. [31], who have surveyed the latest development of electrochemical sensors combined with amplification steps. Additionally, Low et al. [29] have summarised recent advances in nanomaterial-based electrochemical biosensors for detecting different types of miRNAs. It is worth noting that current approaches in this field

often involve complex electrode fabrication using different semiconductors/nanomaterials. Moreover, the methods are labour-intensive and typically require catalytic signal amplification with the use of enzymes to achieve the desired sensitivity for clinical samples. An overview of photoelectrochemical platforms for miRNA detection is presented in Table S1. To overcome the drawbacks of current platforms, the use of singlet oxygen ($^1O_2$)-based photoelectrochemical detection methodology is proposed. The use of photosensitisers generating $^1O_2$ offers an excellent signal-to-noise ratio, enabling the acquisition of a specific response separately from the baseline (matrix) by switching the light on/off [32–35]. Moreover, the proposed methodology uses air instead of internally added reactive reagents or enzymes, which reduces costs, and avoids complex electrode functionalisation.

The new method relies on the hybridisation of the target miRNA with two other shorter DNA probes (capture and detection) in two steps to form a sandwich-like format (Schematic 1 A). The biotinylated DNA capture probe hybridises with half of the target miRNA and binds to streptavidin-coated magnetic beads, whereas the labelled DNA detection probe hybridises with the second half of the target miRNA. The latter contains a $^1O_2$-producing photosensitiser that is detectable by photoelectrochemistry within minutes after the hybridisation (Schematic 1). The photosensitiser chlorine e6 (ChlE6) is selected as a $^1O_2$-producing label [33,36] and hydroquinone (HQ) is chosen as a redox reporter to chemically capture short-lived $^1O_2$ in micrometres-thick layers of the magnetic beads, amplifying the signal rather than the target. Here, for the first time, a $^1O_2$-based photoelectrochemical technology demonstrates the detection of miRNAs in plasma from prostate cancer patients, relevant for clinical diagnostics in addition to clinicopathological information.

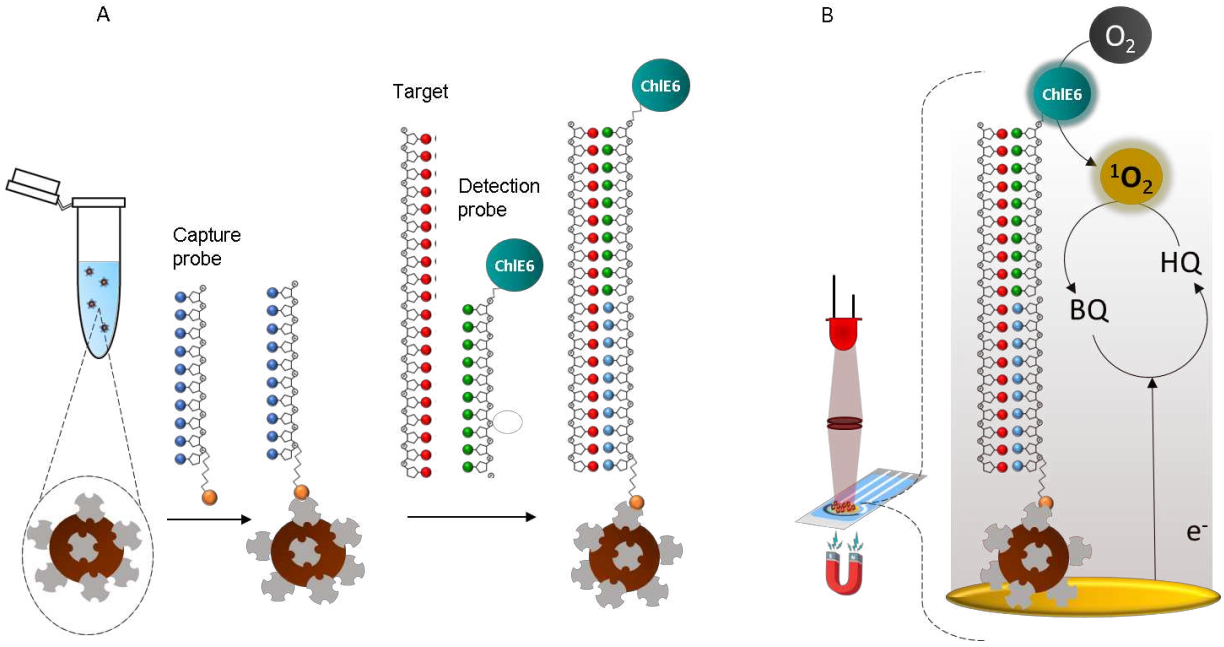

Schematic 1. Schematic representation of (A) the sandwich assay and (B) $^1O_2$-based photoelectrochemical detection of miRNA.

2. MATERIALS AND METHODS

2.1. Reagents

The buffer components (Tris, EDTA (Titriplex III), NaCl, HCl, KH_2PO_4 and KCl) and Tween 20 were purchased from Sigma-Aldrich (Merck, Belgium). HQ was supplied by Acros Organics (Belgium). Streptavidin-coated magnetic beads (M280-Dynabeads) were purchased from Invitrogen (ThermoFischer Scientific, Belgium). Pooled male human plasma (K3 EDTA) was acquired from Bio-connect (The Netherlands). DNA oligonucleotides were used as capture oligonucleotide probes with biotinylated 5' end and as detection oligonucleotide probes (from here on will be known as capture probes and detection probes) with ChlE6 or leuco malachite green (MalG) (type I photosensitiser control) labels. These bind to the complementary target RNA oligonucleotides in a sandwich manner as illustrated in Schematic 1A. The DNA and RNA oligonucleotides were purchased from Eurogentec (Belgium), except for MalG-labelled detection probes which were purchased from Metabion (Germany). MalG-labelled probes were used in the experiments as the type I control photosensitiser. The sequences and modifications of the oligonucleotides are presented in Table S2. The gold-sputtered planar electrodes (AUTR10) were purchased from DropSens (The Netherlands).

2.2. Buffers and solutions

A 2X Tris-EDTA (TE) buffer solution (pH 7.5, adjusted using HCl), containing 10 mM Tris, 1 mM EDTA, and 2 M NaCl was prepared. This 2X TE-buffer was mixed with (i) Tween 20 to yield a 2x TE + 0.05 % Tween 20 (2XTE-T_{20}), or (ii) ultrapure water (UPW, 18.2 MΩ cm^{-1} double deionized water, Sartorius Arium® Ultrapure Water Systems) and Tween 20 to yield a 1xTE + 0.05 % Tween 20 (1XTE-T_{20}) buffer, herein named hybridisation buffer. The measuring buffer with/without HQ at different concentrations (0.01 to 10 mM), consisted of 0.1 M KCl and 0.01 M KH_2PO_4 adjusted to pH 7 with KOH.

2.3. Sandwich hybridisation assay

2.3.1. Hybridisation assay with magnetic beads

Prior to the photoelectrochemical analysis, the target miRNAs were captured and hybridised with capture and detection probes onto the magnetic beads via a sandwich hybridisation assay. First, streptavidin-coated magnetic particles (10 µL, 10 mg/mL, unless stated otherwise) were dispersed in an Eppendorf containing a 1 mL hybridisation buffer (Schematic 1 A). The solution was vortexed and the magnetic beads accumulated at the side of the Eppendorf were directed to the magnetic rack (∼1 min). The solution was removed and the magnetic beads were resuspended in 500 µL of 2XTE-T_{20} buffer, then 500 µL of 100 nM capture probe in UPW+0.05% Tween 20 was added to the beads leading to a final incubation solution containing 1 mL of capture probe at 50 nM in hybridisation buffer. This step lowers the NaCl concentration in the 2X buffer from 2 M to 1 M ensuring optimal binding of the capture probes [37]. This concentration of capture probes was chosen to ensure saturation of all the beads with capture probes, given that the beads have a binding capacity of ~200 pmol of single-stranded oligonucleotides per 1 mg of beads according to the manufacturer's information sheet [37]. This solution was incubated for 15 min at room temperature using continuous rotation (10 rpm, rotary shaker). Following the incubation with capture probes, the beads were again accumulated using a magnetic rack, the solution was discarded and the functionalised beads were resuspended in hybridisation buffer containing the photosensitiser labelled detection probe (24 nM, concentration corresponding to the highest concentration of target used in this study) and target miRNA (at different concentrations between 24 nM and 60 fM). This solution was incubated for 1 hour at room temperature in a rotary shaker at 10 rpm. Following the incubation, the beads were washed three times with 1 mL hybridisation buffer and re-suspended in 10 µL of the same buffer until the photoelectrochemical detection was performed.

Standard curves were constructed with different concentrations (from 24 nM to 60 fM) of target miRNAs in buffer solution while keeping the concentration of detection and capture probes constant at 24 nM and 50 nM, respectively. The specificity of the sensing strategy was evaluated by measuring the photocurrents for different concentrations of target miRNAs in the presence of two other miRNAs (for example, detecting the target miR-141 in the presence of miR-145 and miR-375). Negative control tests were performed using a miRNA (i.e. miR-375) that is not complementary to the capture and detection probes and in the absence of the target miR-141.

Optimisation of parameters and standard curves with plasma (diluted 10-fold with hybridisation buffer) was performed using pooled male human plasma (K3 EDTA). Eight plasma samples from prostate cancer patients in the age group of 62-72 years were obtained from Centro Hospitalar do Porto, Portugal after the appropriate informed consent and approval from The Health Ethics Committee (CES) from Centro Hospitalar do Porto (Ref: 2017.154(131-DEFI/123-CES). Due to the limited quantity of clinical samples, miR-145 was analysed in all samples while miR-141 was analysed in six of the samples.

2.3.2. Chemisorption assay via thiol linking

A comparative analysis was made with a similar sandwich assay where the capture probe was chemisorbed on the surface of the working electrode, via the C6-thiol modification of the 5'-end instead of the biotin-TEG modification. Hereto, electrodes were incubated in a 1 µM thiolated capture probe containing 0.2 µM mercaptohexanol (MH, purity >98.0%, TCI chemicals) in hybridisation buffer (40 µL) overnight (~16 hours) and then in 1 mM MH for 2 h, for backfilling and removing weakly bound DNA molecules. For the hybridisation step, a 40 µL drop consisting of detection probe solution (24 nM) and the target miR-141 (20 nM) in hybridisation buffer was placed on the electrode for 1 h and washed with hybridisation buffer before photoelectrochemical detection.

2.4. $^1O_2$-based photoelectrochemical detection

Following the sandwich hybridisation step, the photoelectrochemical measurements were carried out using a PalmSens4 potentiostat (PalmSens, The Netherlands) using PSTrace 5.9 software or a Metrohm Autolab PGSTAT302N potentiostat (Metrohm, The Netherlands) using Nova 2.1 software. A light-emitting diode (LED) operated at 660 nm (Thorlabs, Inc.) was used and the diameter of the light beam was adjusted using a collimator to only illuminate the working electrode. The light power was adjusted to 30 mW using a PM100D optical power meter (Thorlabs, Inc.). The measurements were performed with 60 s OFF, 10 s ON and 30 s OFF light-chopped conditions for uniformity, with an ON/OFF switch pre-programmed with PSTrace 5.9 or Nova 2.1 and controlled by a relay trigger.

After performing the hybridisation assay, the beads were resuspended in 10 µL of measuring buffer and transferred into the measuring drop (90 µL of measuring buffer placed on the electrode surface), where all the beads precipitated at the working electrode due to a neodymium magnet underneath it. Photocurrents in this setup were measured with reference to. the inbuilt Ag quasi-reference electrode. Polynomial baseline correction was constructed through background current values (in the dark) and subtracted from the chronoamperograms to obtain baseline-corrected photocurrent responses.

3. RESULTS AND DISCUSSION

3.1. Validation of the sensing strategy in buffer

The photoelectrochemical response of the target miRNA hybridised with the capture and detection probes, in a sandwich-like format, was first evaluated. Figure 1 A shows the chronoamperogram under light chopped conditions (light ON periods are shown as light red bars) recorded after hybridising 20 nM target

(miR-141) with the probes, compared to the control experiment without the target miRNA. Measurements were performed in the presence of 10 µM HQ at -0.15 V vs. quasi-internal Ag reference.

Upon illumination, the photocurrent responses in the presence of the target miRNA exceeded 50 times the response of the control. The decay of the photocurrent in time and with the number of illuminations is attributed to nucleic acid cleavages by the photogenerated reactive oxygen species, which is well pronounced for the model DNA-duplexes directly attached to the gold electrode surface via Au-thiol linking [33,38]. Additionally, the photodegradation of ChlE6 might contribute to the decreasing photocurrents [38]. Nevertheless, when the light is switched on, the photocurrent appears near-instantly giving the maximal photocurrent in the first three seconds, while the signal decay shows more sluggish kinetics. Thus, the photocurrent at three seconds after the start of the first illumination will be used as a representative analytical response for the sensing strategy.

Figure 1 B compares the photoelectrochemical responses from the detection of 20 nM miR-141 in the absence and presence of 10 µM HQ from three different scenarios; (i) using magnetic beads, biotinylated capture probe and ChlE6-labelled detection probe; (ii) hybridised directly on gold electrodes using thiolated capture probe and ChlE6-labelled detection probe; (iii) magnetic beads with biotinylated capture probe and detection probe labelled with a chromophore (MalG) that does not generate $^1O_2$. The role of the redox reporter became clear when comparing the photoelectrochemical responses from the detection of 20 nM miR-141 using magnetic beads in the absence and presence of 10 µM HQ. Without HQ, the photocurrent was only 5% of that in the presence of HQ (Figure 1 B, magnetic beads).

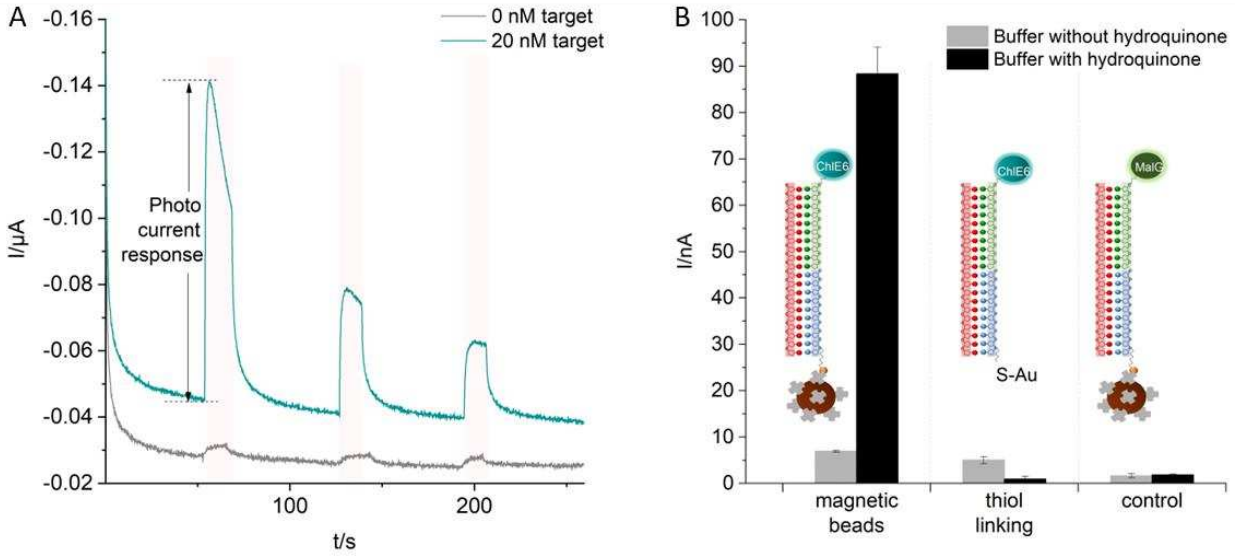

Figure 1. A- Chronoamperogram for the magnetic beads with biotinylated capture probe and ChlE6-labelled detection probe hybridised with miR-141. B- Comparison of photoelectrochemical responses from the detection of 20 nM miR-141 in the absence and presence of 10 µM HQ. Error bars represent the standard deviation (n = 3).

This behaviour agrees with the mechanism in which a comparatively short-lived $^1O_2$ (lifetime ~3.5 µs in water) [39,40] generates the photocurrent. Only 30% of the generated $^1O_2$ can diffuse 100 nm and less than 0.1 % of $^1O_2$ can diffuse more than 200 nm in water [39,40]. Thus, only $^1O_2$ that is generated close to the electrode surface can effectively contribute to the photocurrent in the absence of HQ, whereas most photosensitiser-labelled detection probes on the bead surface (2.8 µm in diameter) will not contribute unless HQ is added into the solution to transform $^1O_2$ into a stable product, benzoquinone (BQ). HQ was

used as the redox reporter to ensure the electron shuttling between all the sites generating $^1O_2$ and the electrode. Thus, HQ is oxidised to BQ on the surface of beads due to the action of $^1O_2$ followed by the reduction of BQ at the electrode to form HQ, making the redox cycle complete (Figure 3 A).

The photocurrent in the absence of HQ (Figure 1 B, magnetic beads) was close to the photocurrent obtained for the same sandwich complex hybridised directly on the gold electrode modified by the thiolated capture probe (Figure 1 B, thiol linking). Noteworthy, HQ does not enhance but suppresses the photocurrent when the detection probe is captured directly at the electrode (Figure 1 B, thiol linking). This can be explained by a relatively fast $^1O_2$ cycloaddition to HQ followed by a slower, rate limiting, molecular reorganisation of the endoperoxide into the peroxide and then BQ (Schematic 2 A). Considering that BQ, but not the endoperoxide, is reduced at the electrode, the resulting photocurrent is smaller compared to photoelectrochemistry obtained for the direct $^1O_2$ reduction (Schematic 2 A). However, HQ does enhance photoelectrochemistry on the magnetic beads (2.8 µm in diameter) since in this case most of $^1O_2$ is generated at distances > 200 nm and cannot contribute to photoelectrochemistry directly.

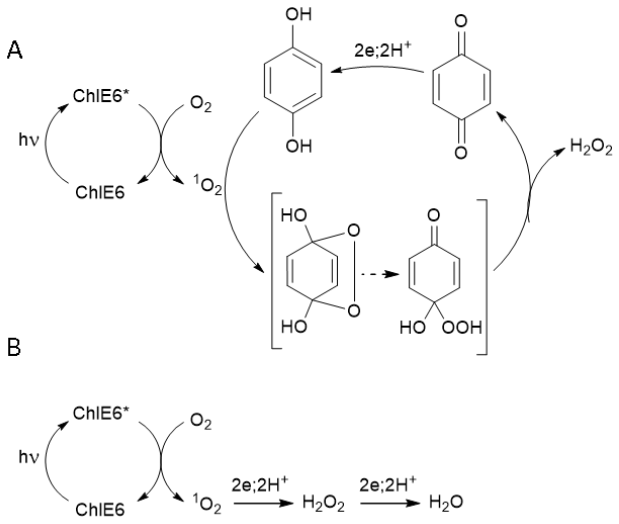

Schematic 2. Photoelectrochemical reaction pathways in the presence(A) and absence(B) of HQ.

Thus, the introduction of magnetic beads resulted in (i) a large surface area available for capturing the target miRNA (e.g. the calculated geometric surface area (GSA) of 100 µg beads is ~ 1.48– 1.72 cm^2 [37], compared to the GSA of AUTR10 is 0.13 cm^2), thus a large effective concentration of the capture probe; (ii) effective mass transfer to the capture probe since the beads are dispersed in the solution and can be stirred in there using rotation; (iii) effective washing from non-bound detection probe (seen from negligible photocurrents in the absence of target); (iv) rapid accumulation of the beads on the sensor surface by a magnet; and (v) sensitive amperometric reading of the molecular label due to redox cycling of HQ/BQ without the need of direct electrical contact between the detection probe and the electrode.

Finally, an alternative chromophore, MalG, which does not generate $^1O_2$ but intensively absorbs the light used (ε_{MalG} is 22000 at 660 nm) and undergoes type I photosensitization mechanism [38] did not produce any noticeable photocurrent in the absence or presence of HQ, when used under the same conditions as for ChlE6 (Figure 1 B, ε_{ChlE6} 12000 at 660 nm) [38] with magnetic beads. This demonstrates that the photocurrents in the absence and presence of HQ are specific to $^1O_2$-generating ChlE6 and not to the beads or other type I ROS/ local heating due to light absorbance by the chromophore.

3.2. Optimisation of working parameters and analytical performance

After demonstrating the photoelectrochemical strategy to detect miRNA using a sandwich assay with magnetic beads, the influence of various working parameters on the assay performance was investigated using miR-141 as the target miRNA. First, the sensor's working potential as a major parameter affecting the sensitivity of the system was optimised (Figure 2). The measurements were performed with 10 µM HQ and 100 µg beads per measurement.

The photocurrent response of the target increases when ranging from +0.05 to -0.2 V but drops at more negative potentials likely due to intense oxygen reduction at the electrode, which is additionally observed as an increase in the dark background current (Figure 2 A). Furthermore, the background reduction of O_2 likely leads to the depletion of available O_2 at the near electrode space and increased formation of superoxide, a known quencher of $^1O_2$ [41]. Hence, the potential of -0.2 V *vs.* quasi-Ag resulted in the maximal response for both 2 nM and 200 nM target miRNA and low blanks and dark current (Figure 2 B), this potential was chosen as the optimal potential and was used in the following experiments.

Next, the optimal quantity of beads used per analysis was determined (Figure 3 A). The measurements were performed with 10 µM HQ at -0.2 V vs quasi-Ag reference. The volume and concentrations of capture and detection probes were kept constant (i.e. 50 nM and 24 nM respectively). An excessive amount of capture and detection probes was provided to saturate all the beads (the optimal amount recommended by the supplier is approximately 200 pmols per mg of beads).

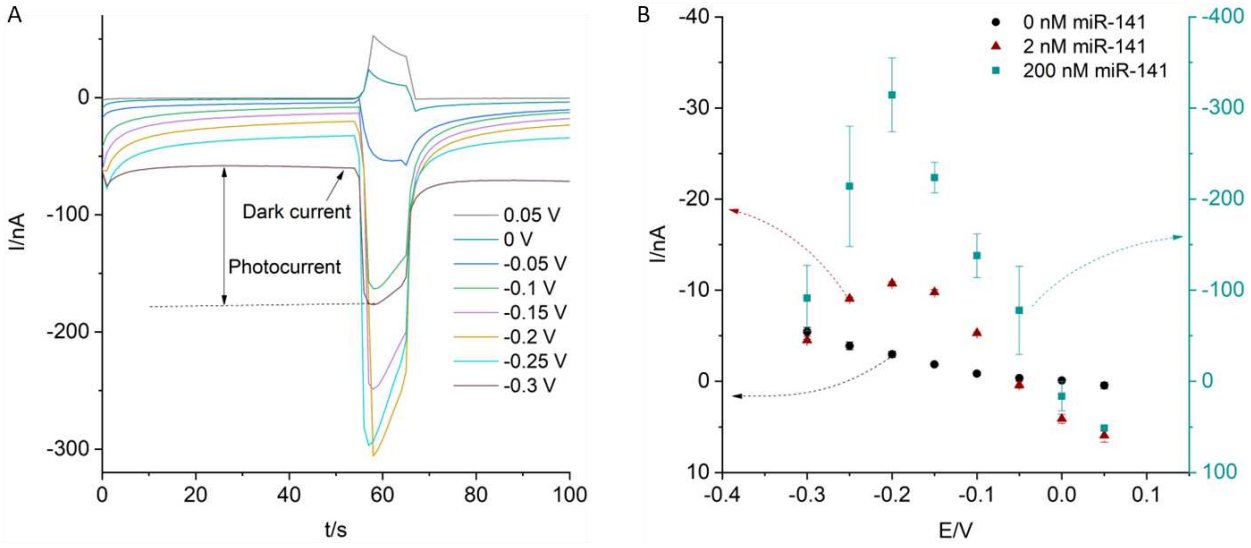

Figure 2. A- Chronoamperograms (raw data without baseline correction) at different electrode potentials in the presence of 20 nM miR-141. B- Dependence of the photocurrent response on the applied electrode potentials. Error bars represent the standard deviation (n = 3).

Maximum response was achieved when using 200 µg of beads for 20 nM target. However, for a lower concentration (0.2 nM) of the target, there was only a 14% increase when using 200 µg instead of 100 µg when compared to the 46% increase for 20 nM target. The decrease in photocurrent response for beads more than 200 µg is likely due to the blocking of light penetration for underlying layers of beads by the first 2-3 layers of beads. This can additionally impede the diffusion of HQ/BQ through the thick layer of beads. Moreover, the standard deviation between repetitions and the background increased to 200 µg compared to 100 µg. Thus, the use of 100 µg of beads was chosen.

Lastly, the effect of the HQ concentration used during the measurements (with 100 µg beads and a potential of -0.2 V vs quasi-Ag reference) was optimised to reach the maximum detectability in the low target concentration range without any amplification. The detectability of a very low concentration, 10 pM of miR-141 compared to the blank control was evaluated at concentrations of HQ ranging from 0.01 to 10 mM (Figure 3 B). The concentration of 1 mM HQ resulted in a response with a high signal-to-noise ratio and demonstrated good reproducibility (standard deviation = 5%) compared to higher HQ concentrations (standard deviation = 22%). We hypothesise that the high standard deviation at the higher concentrations of HQ are attributed to the natural oxidation of HQ in ambient conditions which competes with the kinetics of the photoelectrochemical redox cycle. Thus, 1 mM HQ was chosen as the optimal redox reporter concentration for further studies. With these optimised parameters, control experiments were performed with only detection probe and target miR-141 (D/T), only capture probe and target miR-141 (C/T) and with only capture and detection probe (C/D). This was compared with the signal when the target was present in the system along with the capture and detection probe (C/D/T) (Figure S1). In the absence of either capture, detection probe, or target, the sandwich duplex did not form, thus no noticeable signal was obtained.

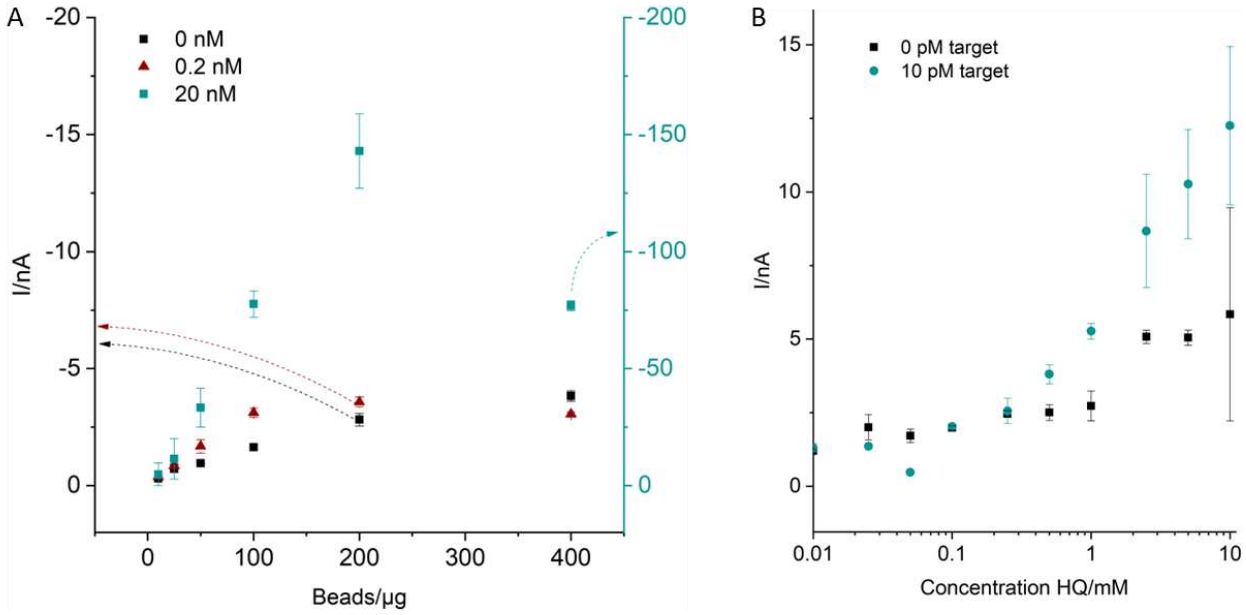

Figure 3. A- Effect of magnetic beads quantity used per analysis. B- Effect of HQ concentration used in the measuring buffer. Error bars represent the standard deviation (n = 3).

Following the optimisation of the assay, the analytical performance of the sensing strategy has been evaluated in buffer solution with the optimised parameters (amount of beads per analysis: 100 µg; potential: -0.2 V vs quasi-Ag reference; HQ concentration: 1 mM).

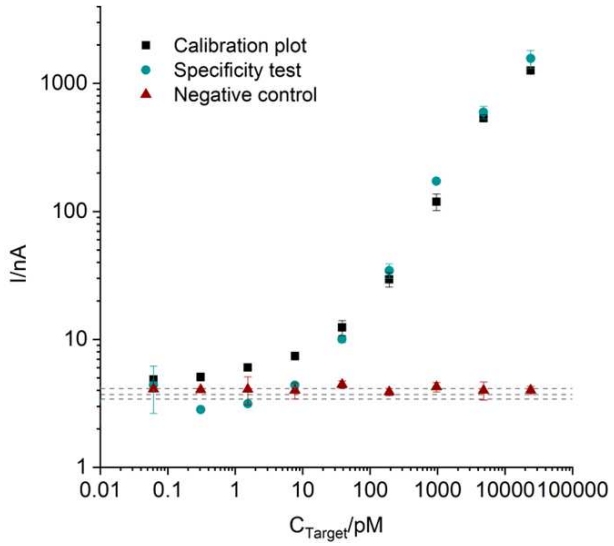

Figure 4. Photoelectrochemical detection of miR-145 in hybridisation buffer with optimised parameters. Reference lines indicate the photocurrent responses in the absence of target. Error bars represent the standard deviation (n = 3).

Figure 4 shows the calibration plots for miR-141 in the concentration range from 0.06 pM to 10 nM (5-fold serial dilution of the target), including two controls. The limit of detection was calculated to be 0.62 pM, calculated from the slope (117 nA/nM, LOD =3*S.D_{blank}/slope [42]) of the calibration curve in the range 0.31 pM – 1 nM, 1.5 pM was the lowest tested concentration that significantly differed from the blanks. The first control tests specificity by measuring the different concentrations of miR-141 in a mixture with 24 nM of two other miRNAs (miR-145 and miR-375). The method demonstrates good specificity with a photocurrent response proportional to the concentration of miR-141 despite the presence of the other targets. In the second control (negative control), the concentration of a target (in this case, miR-375) not complementary to the capture and detection probes, was varied in the same range and resulted in negligible photocurrents similar to blanks (0 pM target).

3.3. Matrix effect

The ability of the system to detect miRNAs in clinically relevant sample matrices ensures future uptake of the sensing technology. Plasma and serum are often the matrices of interest for clinical applications. The photocurrent responses of 10 pM miR-141 spiked in serum and plasma (both 1:20 diluted in buffer) were compared to the response obtained in a buffer solution (Figure 5). The 1:20 dilution was chosen based on our previous investigations for miRNA detection in human serum using the electrochemiluminescence technique [43].

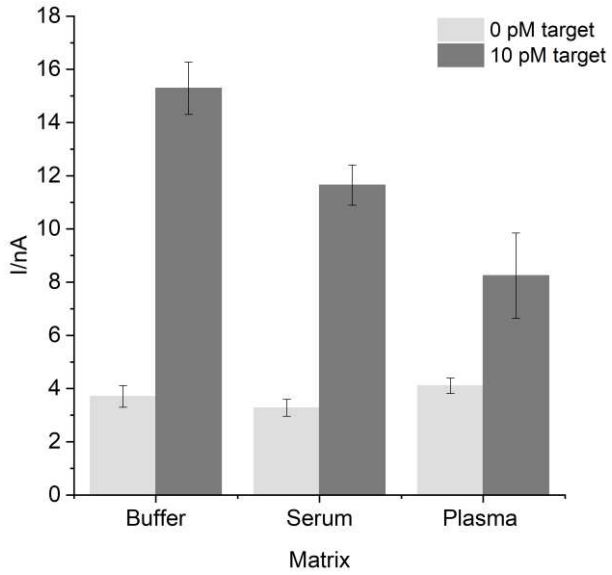

Figure 5. Photoelectrochemical responses from miR-141 in different matrices. Error bars represent the standard deviation (n = 3).

The photocurrent response decreased by 24% in serum, similar to the 26% previously observed in an electrochemiluminescent assay [43] and by 59% in plasma in agreement with the complexity of the matrices. The blank responses (0 pM target) from serum, and plasma are within the standard deviation of the photocurrents in the buffer. Also, there were no false positives due to the complexity of the serum or plasma matrices. However, the specific response decreased due to the matrix effect, which is expected due to the interference from proteins in serum and plasma, lowering the interaction between DNA probes and miRNA due to steric hindrance effects [44]. Nevertheless, 10 pM miR-141 in plasma could be detected suggesting further applicability of the assays in POC devices without the need for sample processing, such as nucleic acid extraction. To ensure the lowest contribution of the matrix on the photocurrent, the effects of the plasma dilution and the incubation time on the photocurrent response of the target were studied by spiking miRNA in commercially available pooled plasma from healthy men (supplementary section, Figure S2). A 10-fold plasma dilution and one hour incubation time was selected for further experiments with plasma. Nevertheless, the results obtained with 15 minutes of incubation showed that when a quick diagnostic test is required aiming for POC analysis, the time of analysis might be shortened.

3.4. Analysis of plasma samples from prostate cancer patients

The applicability of the sensing strategy to evaluate clinical samples was demonstrated through the analysis of samples from prostate cancer patients receiving treatment at Centro Hospitalar Universitário do Porto in Portugal. To compare and estimate the levels of miR-145 and miR-141 in patient samples, standard curves with optimised parameters were constructed by spiking different concentrations (between 1.5 pM and 24 nM, 5-fold serial dilution of the target) of miRNAs in commercially available pooled plasma from healthy men, 10-fold diluted (Figure 6 A). A detection limit of 3.5 pM and 8.3 pM was achieved for miR-145 and miR-141, respectively (Table S3).

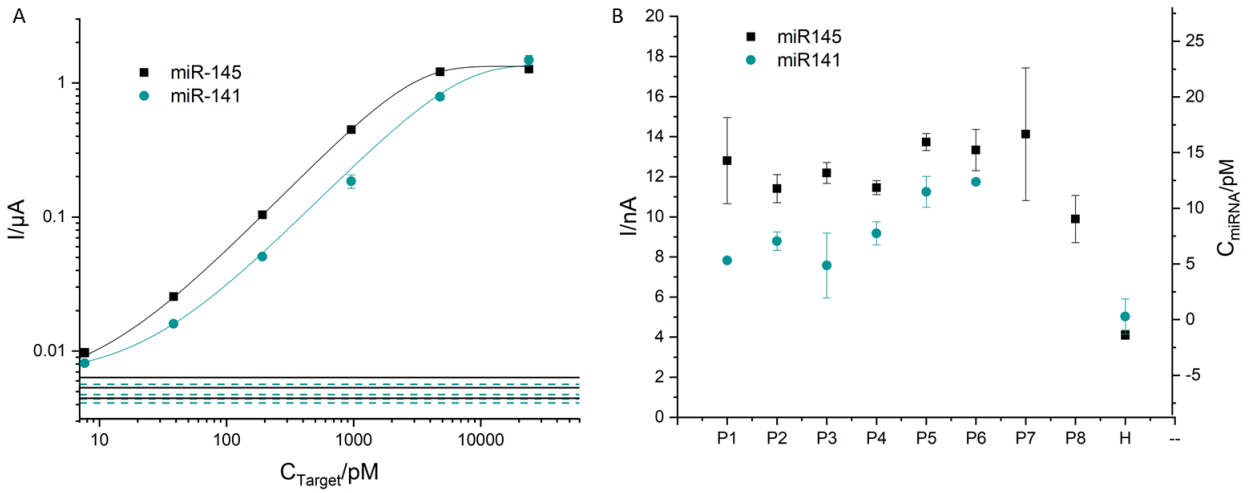

Figure 6. A- Standard curve constructed with healthy male pooled plasma spiked with different concentrations of miR-145 and miR-141. Solid and dashed reference lines indicate the photocurrent response in the absence of target miR-145 and miR-141 respectively. B- Photocurrent responses and calculated concentrations of miRNAs from prostate cancer patient samples (P1-P8). Pooled plasma from healthy men 'H' was included as a control. Error bars represent the standard deviation (n = 3).

Analysis was done for plasma samples derived from eight patients (P1-P8) with prostate cancer (clinicopathological characteristics depicted in Table S4). These plasma samples from prostate cancer subjects have been obtained using the protocol mentioned in the supplementary section. Due to the differences in the patient sample volume, all the plasma samples (P1-P8) were analysed for the most relevant miR-145 [15] and six samples (P1-P6) were analysed for miR-141, all diluted 10-fold (Figure 6 B).

As depicted in Figure 6 B, all the patient samples exhibited different photocurrent responses in the range of 8 – 18 nA, all higher than the response from the pooled healthy male plasma which was between 4.5 – 5.5 nA (considering both miR-141 and miR-145). Photocurrents from the patient plasma samples were converted into miRNA concentrations using the slope of the calibration plot (Figure 6 B, Table 1). Results correlate well with the expected higher expression of miR-141 and miR-145 in prostate cancer patients, as reported in the literature [15,16,45–49].

Table 1. Concentrations of miRNAs calculated for non-diluted patient samples in this study with photoelectrochemistry.

	Calculated levels of miRNA	
	miR-145 (pM)	miR-141 (pM)
P1	145 ± 41	59 ± 4
P2	118 ± 14	98 ± 18
P3	133 ± 10	69 ± 36
P4	119 ± 7	113 ± 23
P5	163 ± 8	196 ± 31
P6	155 ± 20	215 ± 3

P7	171 ± 64	-
P8	89 ± 23	-

Interestingly, the photocurrents and, thus, the concentration of miR-145 in patient samples were always higher and varied less compared to miR-141. Although, a larger study is needed to include blank control samples from healthy individuals to better assess variability in miRNA levels in patients and control groups, or by following up with patients to ascertain whether they present disease progression [14]. To the best of our knowledge, there is no consensus in the literature about the exact levels of miRNAs in plasma since most reports do not use absolute quantification, making it difficult to compare the obtained concentrations with the literature [50].

The conventional miRNA detection protocols typically include pre-amplification, dilution and detection steps, thus requiring careful data normalisation to interpret relative changes in miRNA levels [51]. Our assay offers specific and sensitive miRNA detection in untreated plasma without any pre-amplification steps, which is straightforward for interpretation and may provide better knowledge regarding variations and dysregulation in levels of circulating miRNAs, opening new opportunities for POC usage.

4. CONCLUSIONS

This work describes a PCR-free $^1O_2$-based photoelectrochemical method for quantifying miRNA in plasma samples. The method combines the usability of (i) magnetic beads to capture target miRNA from a complex matrix such as plasma and (ii) our original concept of employing $^1O_2$ in photoelectrochemical sensing for robust and sensitive detection and quantification. We were able to quantitatively measure miRNAs in medical samples from prostate cancer patients with a low-cost electrochemical setup equipped using a LED and without the need for additional PCR or other amplification techniques. Furthermore, this strategy can also be extended to other DNA/RNA sequences by simply choosing different capture and detection probes. Additionally, the underlying methodology can be extended to multiplex platforms using commercially available multi-array electrode platforms (e.g. 96-well plates) modified with a system for photoexcitation. However, miniaturisation of the LEDs and careful fabrication of the setup is essential for the multiplexed detection of miRNA panels. This makes our detection method relevant for liquid biopsy applications, demonstrating the general feasibility and clinical relevance in nucleic acid-based diagnostics.

ACKNOWLEDGMENTS

This work was supported by the Special Research Fund of the University of Antwerp [grant numbers iBOF/23/030, BOF DOCPRO and BOF SEP]; the Marie Skłodowska-Curie Actions [MSCA-IF grant number 842219 to RC]; and the Research Foundation – Flanders (FWO) [grant numbers G054819N and 1256424N to ED].

SUPPLEMENTARY MATERIAL

Supplementary data to this article can be found online.

REFERENCES

[1] H. Sung, J. Ferlay, R.L. Siegel, M. Laversanne, I. Soerjomataram, A. Jemal, F. Bray, Global Cancer Statistics 2020: GLOBOCAN Estimates of Incidence and Mortality Worldwide for 36 Cancers in 185 Countries, CA Cancer J Clin 71 (2021) 209–249. https://doi.org/https://doi.org/10.3322/caac.21660.

[2] G. Poulet, J. Massias, V. Taly, Liquid Biopsy: General Concepts, Acta Cytol 63 (2019) 449–455. https://doi.org/10.1159/000499337.
[3] H. Schwarzenbach, D.S.B. Hoon, K. Pantel, Cell-free nucleic acids as biomarkers in cancer patients, Nat Rev Cancer 11 (2011) 426–437. https://doi.org/10.1038/nrc3066.
[4] V. Akpe, T.H. Kim, C.L. Brown, I.E. Cock, Circulating tumour cells: a broad perspective, J R Soc Interface 17 (2020) 20200065. https://doi.org/10.1098/rsif.2020.0065.
[5] C. Han Li, Y. Chen, Small and Long Non-Coding RNAs: Novel Targets in Perspective Cancer Therapy, in: Curr Genomics, Bentham Science Publishers, 2015: pp. 319–326.
[6] M.A. Jafri, M.H. Al-Qahtani, J.W. Shay, Role of miRNAs in human cancer metastasis: Implications for therapeutic intervention, Semin Cancer Biol 44 (2017) 117–131. https://doi.org/https://doi.org/10.1016/j.semcancer.2017.02.004.
[7] M.C. Maia, M. Salgia, S.K. Pal, Harnessing cell-free DNA: plasma circulating tumour DNA for liquid biopsy in genitourinary cancers, Nat Rev Urol 17 (2020) 271–291. https://doi.org/10.1038/s41585-020-0297-9.
[8] L. Fabris, Y. Ceder, A.M. Chinnaiyan, G.W. Jenster, K.D. Sorensen, S. Tomlins, T. Visakorpi, G.A. Calin, The Potential of MicroRNAs as Prostate Cancer Biomarkers, Eur Urol 70 (2016) 312–322. https://doi.org/https://doi.org/10.1016/j.eururo.2015.12.054.
[9] D. Vanacore, M. Boccellino, S. Rossetti, C. Cavaliere, C. D'aniello, R. Di Franco, F.J. Romano, M. Montanari, E. La Mantia, R. Piscitelli, F. Nocerino, F. Cappuccio, G. Grimaldi, A. Izzo, L. Castaldo, M.F. Pepe, M.G. Malzone, G. Iovane, G. Ametrano, P. Stiuso, L. Quagliuolo, D. Barberio, S. Perdonà, P. Muto, M. Montella, P. Maiolino, B.M. Veneziani, G. Botti, M. Caraglia, G. Facchini, Micrornas in prostate cancer: an overview, Oncotarget 8 (2017) 50240–50251. www.impactjournals.com/oncotarget/.
[10] R. Tavallaie, S.R.M. De Almeida, J.J. Gooding, Toward biosensors for the detection of circulating microRNA as a cancer biomarker: an overview of the challenges and successes, WIREs Nanomedicine and Nanobiotechnology 7 (2015) 580–592. https://doi.org/https://doi.org/10.1002/wnan.1324.
[11] J.C. Brase, M. Johannes, T. Schlomm, M. Fälth, A. Haese, T. Steuber, T. Beissbarth, R. Kuner, H. Sültmann, Circulating miRNAs are correlated with tumor progression in prostate cancer, Int J Cancer 128 (2011) 608–616. https://doi.org/https://doi.org/10.1002/ijc.25376.
[12] A. Sita-Lumsden, C.E. Fletcher, D.A. Dart, G.N. Brooke, J. Waxman, C.L. Bevan, Circulating nucleic acids as biomarkers of prostate cancer, Biomark Med 7 (2013) 867–877. https://doi.org/10.2217/bmm.13.104.
[13] V. Mugoni, Y. Ciani, C. Nardella, F. Demichelis, Circulating RNAs in prostate cancer patients, Cancer Lett 524 (2022) 57–69. https://doi.org/https://doi.org/10.1016/j.canlet.2021.10.011.
[14] S. Rana, G.N. Valbuena, E. Curry, C.L. Bevan, H.C. Keun, MicroRNAs as biomarkers for prostate cancer prognosis: a systematic review and a systematic reanalysis of public data, Br J Cancer 126 (2022) 502–513. https://doi.org/10.1038/s41416-021-01677-3.
[15] J. Shen, G.W. Hruby, J.M. McKiernan, I. Gurvich, M.J. Lipsky, M.C. Benson, R.M. Santella, Dysregulation of circulating microRNAs and prediction of aggressive prostate cancer, Prostate 72 (2012) 1469–1477. https://doi.org/https://doi.org/10.1002/pros.22499.
[16] Y. Xu, S. Qin, T. An, Y. Tang, Y. Huang, L. Zheng, MiR-145 detection in urinary extracellular vesicles increase diagnostic efficiency of prostate cancer based on hydrostatic filtration dialysis method, Prostate 77 (2017) 1167–1175. https://doi.org/https://doi.org/10.1002/pros.23376.
[17] C. Chen, D.A. Ridzon, A.J. Broomer, Z. Zhou, D.H. Lee, J.T. Nguyen, M. Barbisin, N.L. Xu, V.R. Mahuvakar, M.R. Andersen, K.Q. Lao, K.J. Livak, K.J. Guegler, Real-time quantification of microRNAs by stem–loop RT–PCR, Nucleic Acids Res 33 (2005) e179–e179. https://doi.org/10.1093/nar/gni178.

[18] C. Chen, R. Tan, L. Wong, R. Fekete, J. Halsey, Quantitation of MicroRNAs by Real-Time RT-qPCR, in: D.J. Park (Ed.), PCR Protocols, Humana Press, Totowa, NJ, 2011: pp. 113–134. https://doi.org/10.1007/978-1-60761-944-4_8.

[19] Y. Hu, W. Lan, D. Miller, Next-Generation Sequencing for MicroRNA Expression Profile, in: J. Huang, G.M. Borchert, D. Dou, J. (Luke) Huan, W. Lan, M. Tan, B. Wu (Eds.), Bioinformatics in MicroRNA Research, Springer New York, New York, NY, 2017: pp. 169–177. https://doi.org/10.1007/978-1-4939-7046-9_12.

[20] E. Miotto, E. Saccenti, L. Lupini, E. Callegari, M. Negrini, M. Ferracin, Quantification of Circulating miRNAs by Droplet Digital PCR: Comparison of EvaGreen- and TaqMan-Based Chemistries, Cancer Epidemiology, Biomarkers & Prevention 23 (2014) 2638–2642. https://doi.org/10.1158/1055-9965.EPI-14-0503.

[21] L. Moldovan, K.E. Batte, J. Trgovcich, J. Wisler, C.B. Marsh, M. Piper, Methodological challenges in utilizing miRNAs as circulating biomarkers, J Cell Mol Med 18 (2014) 371–390. https://doi.org/https://doi.org/10.1111/jcmm.12236.

[22] E.E. Ferapontova, DNA Electrochemistry and Electrochemical Sensors for Nucleic Acids, Annual Review of Analytical Chemistry 11 (2018) 197–218. https://doi.org/10.1146/annurev-anchem-061417-125811.

[23] P. Gillespie, S. Ladame, D. O'Hare, Molecular methods in electrochemical microRNA detection, Analyst 144 (2019) 114–129. https://doi.org/10.1039/C8AN01572D.

[24] J.I.A. Rashid, N.A. Yusof, The strategies of DNA immobilization and hybridization detection mechanism in the construction of electrochemical DNA sensor: A review, Sens Biosensing Res 16 (2017) 19–31. https://doi.org/https://doi.org/10.1016/j.sbsr.2017.09.001.

[25] K.S. V Santhanam, Electrochemical approaches towards sensing viruses: A mini review, Med Devices Sens 4 (2021) e10148. https://doi.org/https://doi.org/10.1002/mds3.10148.

[26] P.S. Sfragano, S. Pillozzi, I. Palchetti, Electrochemical and PEC platforms for miRNA and other epigenetic markers of cancer diseases: Recent updates, Electrochem Commun 124 (2021) 106929. https://doi.org/https://doi.org/10.1016/j.elecom.2021.106929.

[27] S. Thiruvottriyur Shanmugam, S. Trashin, K. De Wael, Gold-sputtered microelectrodes with built-in gold reference and counter electrodes for electrochemical DNA detection, Analyst 145 (2020) 7646–7653. https://doi.org/10.1039/D0AN01387K.

[28] M. El Aamri, G. Yammouri, H. Mohammadi, A. Amine, H. Korri-Youssoufi, Electrochemical Biosensors for Detection of MicroRNA as a Cancer Biomarker: Pros and Cons, Biosensors (Basel) 10 (2020) 186. https://doi.org/10.3390/bios10110186.

[29] S.L. Low, Y.S. Leo, Y.L. Lai, S. Lam, H.H. Tan, J.C.C. Wong, L.K. Tan, L.C. Ng, Evaluation of eight commercial Zika virus IgM and IgG serology assays for diagnostics and research, PLoS One 16 (2021) e0244601. https://doi.org/10.1371/journal.pone.0244601.

[30] M. Tabata, Y. Miyahara, Liquid biopsy in combination with solid-state electrochemical sensors and nucleic acid amplification, J Mater Chem B 7 (2019) 6655–6669. https://doi.org/10.1039/C9TB00718K.

[31] P. Gillespie, R.B. Channon, X. Meng, M.N. Islam, S. Ladame, D. O'Hare, Nucleic acid sensing via electrochemical oligonucleotide-templated reactions, Biosens Bioelectron 176 (2021) 112891. https://doi.org/https://doi.org/10.1016/j.bios.2020.112891.

[32] S. Trashin, F. Morales-Yánez, S. Thiruvottriyur Shanmugam, L. Paredis, E.N. Carrión, I. Sariego, S. Muyldermans, K. Polman, S.M. Gorun, K. De Wael, Nanobody-Based Immunosensor Detection Enhanced by Photocatalytic-Electrochemical Redox Cycling, Anal Chem 93 (2021) 13606–13614. https://doi.org/10.1021/acs.analchem.1c02876.

[33] S. Trashin, V. Rahemi, K. Ramji, L. Neven, S.M. Gorun, K. De Wael, Singlet oxygen-based electrosensing by molecular photosensitizers, Nat Commun 8 (2017) 16108. https://doi.org/10.1038/ncomms16108.

[34] E. Daems, S. Bassini, L. Mariën, H. Op de Beeck, A. Stratulat, K. Zwaenepoel, T. Vandamme, K. Op de Beeck, S. Koljenović, M. Peeters, G. Van Camp, K. De Wael, Singlet oxygen-based photoelectrochemical detection of single-point mutations in the KRAS oncogene, Biosens Bioelectron 249 (2024) 115957. https://doi.org/https://doi.org/10.1016/j.bios.2023.115957.

[35] M. Verrucchi, G.E. Giacomazzo, P.S. Sfragano, S. Laschi, L. Conti, M. Pagliai, C. Gellini, M. Ricci, E. Ravera, B. Valtancoli, C. Giorgi, I. Palchetti, Characterization of a Ruthenium(II) Complex in Singlet Oxygen-Mediated Photoelectrochemical Sensing, Langmuir 39 (2023) 679–689. https://doi.org/10.1021/acs.langmuir.2c03042.

[36] S.U. Khan, S.A. Trashin, Y.S. Korostei, T. V Dubinina, L.G. Tomilova, S.W. Verbruggen, K. De Wael, Photoelectrochemistry for Measuring the Photocatalytic Activity of Soluble Photosensitizers, ChemPhotoChem 4 (2020) 300–306. https://doi.org/https://doi.org/10.1002/cptc.201900275.

[37] Invitrogen, Dynabeads™ M-280 Streptavidin, 2018. www.thermofisher.com/us/en/home/global/.

[38] S.T. Shanmugam, S. Trashin, K. De Wael, Singlet oxygen-based photoelectrochemical detection of DNA, Biosens Bioelectron 195 (2022) 113652. https://doi.org/https://doi.org/10.1016/j.bios.2021.113652.

[39] D.E. Latch, K. McNeill, Microheterogeneity of Singlet Oxygen Distributions in Irradiated Humic Acid Solutions, Science (1979) 311 (2006) 1743–1747. https://doi.org/10.1126/science.1121636.

[40] F. Wilkinson, W.P. Helman, A.B. Ross, Rate Constants for the Decay and Reactions of the Lowest Electronically Excited Singlet State of Molecular Oxygen in Solution. An Expanded and Revised Compilation, J Phys Chem Ref Data 24 (1995) 663–677. https://doi.org/10.1063/1.555965.

[41] H.J. Guiraud, C.S. Foote, Chemistry of superoxide ion. III. Quenching of singlet oxygen, J Am Chem Soc 98 (1976) 1984–1986. https://doi.org/10.1021/ja00423a066.

[42] P. Borman, D. Elder, Q2(R1) Validation of Analytical Procedures, in: ICH Quality Guidelines, 2017: pp. 127–166. https://doi.org/https://doi.org/10.1002/9781118971147.ch5.

[43] R. Campos, S.T. Shanmugam, E. Daems, R. Ribeiro, K. De Wael, Development of an electrochemiluminescent oligonucleotide-based assay for the quantification of prostate cancer associated miR-141-3p in human serum, Bioelectrochemistry 153 (2023) 108495. https://doi.org/https://doi.org/10.1016/j.bioelechem.2023.108495.

[44] S.S. Mahshid, S. Camiré, F. Ricci, A. Vallée-Bélisle, A Highly Selective Electrochemical DNA-Based Sensor That Employs Steric Hindrance Effects to Detect Proteins Directly in Whole Blood, J Am Chem Soc 137 (2015) 15596–15599. https://doi.org/10.1021/jacs.5b04942.

[45] H.H. Cheng, P.S. Mitchell, E.M. Kroh, A.E. Dowell, L. Chéry, J. Siddiqui, P.S. Nelson, R.L. Vessella, B.S. Knudsen, A.M. Chinnaiyan, K.J. Pienta, C. Morrissey, M. Tewari, Circulating microRNA Profiling Identifies a Subset of Metastatic Prostate Cancer Patients with Evidence of Cancer-Associated Hypoxia, PLoS One 8 (2013) e69239-. https://doi.org/10.1371/journal.pone.0069239.

[46] H.C.N. Nguyen, W. Xie, M. Yang, C.-L. Hsieh, S. Drouin, G.-S.M. Lee, P.W. Kantoff, Expression differences of circulating microRNAs in metastatic castration resistant prostate cancer and low-risk, localized prostate cancer, Prostate 73 (2013) 346–354. https://doi.org/https://doi.org/10.1002/pros.22572.

[47] P. Porzycki, E. Ciszkowicz, M. Semik, M. Tyrka, Combination of three miRNA (miR-141, miR-21, and miR-375) as potential diagnostic tool for prostate cancer recognition, Int Urol Nephrol 50 (2018) 1619–1626. https://doi.org/10.1007/s11255-018-1938-2.

[48] H.L. Zhang, X.J. Qin, D.L. Cao, Y. Zhu, X.D. Yao, S.L. Zhang, B. Dai, D.W. Ye, An elevated serum miR-141 level in patients with bone-metastatic prostate cancer is correlated with more bone lesions, Asian J Androl 15 (2013) 231–235. https://doi.org/10.1038/aja.2012.116.

[49] I.A. Paunescu, R. Bardan, A. Marcu, D. Nitusca, A. Dema, S. Negru, O. Balacescu, L. Balacescu, A. Cumpanas, I.O. Sirbu, B. Petrut, E. Seclaman, C. Marian, Biomarker potential of plasma microRNA-150-5p in prostate cancer, Medicina (B Aires) 55 (2019). https://doi.org/10.3390/medicina55090564.

[50] A.F. Jou, C.-H. Lu, Y.-C. Ou, S.-S. Wang, S.-L. Hsu, I. Willner, J.A. Ho, Diagnosing the miR-141 prostate cancer biomarker using nucleic acid-functionalized CdSe/ZnS QDs and telomerase, Chem Sci 6 (2015) 659–665. https://doi.org/10.1039/C4SC02104E.

[51] A.B. Gevaert, I. Witvrouwen, C.J. Vrints, H. Heidbuchel, E.M. Van Craenenbroeck, S.J. Van Laere, A.H. Van Craenenbroeck, MicroRNA profiling in plasma samples using qPCR arrays: Recommendations for correct analysis and interpretation, PLoS One 13 (2018) e0193173-. https://doi.org/10.1371/journal.pone.0193173.